ACI STRUCTURAL JOURNAL TECHNICAL PAPER

MS No. S-2018-529.R2

Experimental Evaluation and Modeling of Corroded Reinforced Concrete Columns

by Hakan Yalciner and Atila Kumbasaroglu

A total of 30 full-scale reinforced concrete (RC) columns were tested to develop models for the prediction of the structural behavior of corroded RC columns. Of these, 25 RC columns were tested under cyclic loading for two different applied axial load ratios—namely, 0.20 and 0.40—at three concrete strength levels—namely, 9, 27, and 37 MPa (1305, 3915, and 5365 psi)—and at four corrosion levels. Five RC columns were loaded monotonically with an axial load ratio of 0.20 at four corrosion levels to calculate the damage index. The actual corrosion levels were obtained by breaking the concrete and extracting all the reinforcing bars. The test results demonstrated that the ductility ratios of the corroded RC columns, which were not determined in accordance with energy-based or bilateral failure criteria, could be misleading. The determined energy dissipation capacity and damage index of the columns further revealed the corrosion effects.

Keywords: assessment; column; corrosion; reinforcement bar; seismic.

INTRODUCTION

The accurate prediction of the structural behavior of corroded reinforced concrete (RC) buildings can be achieved by modeling the materials affected by corrosion and by performing nonlinear analysis using modified plastic hinge properties. One of the major effects of corrosion that reduces the seismic performance levels of RC structures is reduction in the cross-sectional area of the reinforcement bars. A reduction in RC structure performance levels does not depend only on losing a cross-sectional area of the reinforcement bars (Yalciner et al. 2015). Other effects of corrosion such as cracking of concrete, reduction in bond strength, and the mechanical properties of concrete and steel bars may also cause reduction in the seismic performance levels of RC structures. Owing to the unknowns and difficulties involved in corrosion, its effects are generally preferred to be considered as the reduction in the cross-sectional area of reinforcement bars for decision making on the seismic performance levels of existing RC buildings, unless detailed information is collected from the existing structures and its effects are fully considered (for example, mechanical properties of materials, bond-slip relationships, and confinement effects). Structural data obtained from experimental studies on corroded RC members provide easier and more practical approaches for the structural assessment of corroded RC buildings. Thus, numerous experimental studies have been conducted to examine the effects of corrosion on RC columns, as summarized in Table 1. One of the experimental studies on the prediction of the structural behavior of corroded RC columns was conducted by Ma et al. (2012). In that study, the applied axial load ratios were increased with corrosion level. Another experimental study to evaluate structural behavior of the corroded RC columns was performed by Meda et al. (2014). In the study done by Meda et al. (2014), stirrups were coated and the longitudinal bars were corroded as the third level of the columns. Thus, the bond strength degradation owing to the corrosion of the stirrups and contribution of stirrups to the lateral displacement were neglected. In contrast to Ma et al. (2012) and Meda et al. (2014), Guo et al. (2015) obtained the actual corrosion levels at both the longitudinal bars and stirrups. Yang et al. (2016) noted that the ductility ratios of the RC columns decreased as the corrosion level increased. By contrast, the ductility ratio of each corroded RC column increased for each corrosion level in Li et al. (2018), and up to a certain corrosion level in Ma et al. (2012) and Guo et al. (2015). Although several experimental results indicated an increase in the ductility ratio (Guo et al. 2015; Li et al. 2018) and energy dissipation (Ma et al. 2012; Meda et al. 2014) of corroded RC columns in comparison with non-corroded columns, other studies reported a reduction in the ductility ratio (Ma et al. 2012; Yang et al. 2016) and energy dissipation (Guo et al. 2015; Yang et al. 2016; Liu et al. 2017; Yuan et al. 2017).

RESEARCH SIGNIFICANCE

Currently, there exist few models for predicting the seismic performance of corroded RC columns. Contradicting results have been obtained regarding the ductility ratio and energy dissipation capacity of corroded RC columns owing the limited dependent variables (that is, the same concrete strength level or axial load ratio were used) and considered failure criteria. In contrast to previous studies, in the present study, 30 RC columns were evaluated at three different concrete strength levels, different corrosion levels, and for two axial loads. The corrosion levels were specifically designed to investigate the contradicting results reported in various studies.

EXPERIMENTAL PROGRAM

The test specimens were first divided into three main groups for three different concrete strength levels—namely, C8, C20, and C30. Each group was then divided into four subgroups for different corrosion levels. Thereafter, each subgroup was tested for two different applied axial loads of 20 and 40% under cyclic loading. The specimens were

ACI Structural Journal, V. 117, No. 4, July 2020.

MS No. S-2018-529.R2, doi: 10.14359/51721372, received June 6, 2019, and reviewed under Institute publication policies. Copyright © 2020, American Concrete Institute. All rights reserved, including the making of copies unless permission is obtained from the copyright proprietors. Pertinent discussion including author's closure, if any, will be published ten months from this journal's date if the discussion is received within four months of the paper's print publication.

Table 1—Summarized studies

Previous studies	Ma et al. (2012)	Meda et al. (2014)	Guo et al. (2015)	Yang et al. (2016)	Li et al. (2018)
Number of specimens	13	2	4	5	6
Axial load ratio	0.15 to 0.90	0.22	0.10	0.18	0.10 and 0.30
$f_{c\text{-}cubic}$, MPa (psi)	32.4 (4698)	20 (2900)	42.9 (6220.5)	46.4 (6728)	50.2 (7279)
Obtained corrosion levels	Actual corrosion levels	Faraday's mass loss	Actual corrosion levels	Actual corrosion levels	Actual corrosion levels
CL_L, %	0 to 15.1	20	5, 10, and 15	0 to 16.8	0 to 18.45
Considered corrosion levels	Average corrosion levels	Faraday's mass loss	Average corrosion levels	Maximum corrosion levels	Average corrosion levels
μ_D	Increased for corrosion levels of 4.1 and 9.5% with axial load ratios of 0.25 and 0.15, respectively	Increased for a corrosion level of 20%	Increased for a corrosion level of 5.07%	Decreased for each corrosion level	Increased for each corrosion level
E	Increased for a corrosion level of 14%	Decreased for a corrosion level of 20%	Decreased for each corrosion level	Decreased for each corrosion level	Decreased for each corrosion level
Developed models	Yield and ultimate loads, displacement ductility ratio and stiffness degradation	—	—	Displacement ductility ratio and energy absorption	—

Note: $f_{c\text{-}cubic}$ is cubic concrete compressive strength; CL_L is corrosion levels of longitudinal bars; μ_D is displacement ductility ratio; E is energy dissipation capacity.

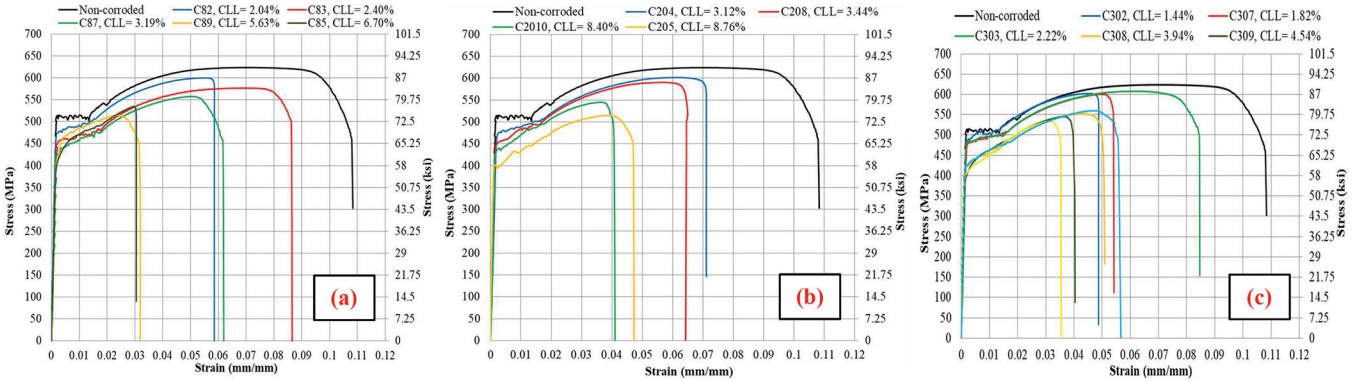


Fig. 1—Mechanical properties of corroded bars: (a) C8; (b) C20; and (c) C30.

designated as $CA_{B,\ \%x,\ \%y,\ z}$, where A indicates the concrete strength level; B indicates the number of specimens; x and y represent the average corrosion levels of the longitudinal bars and stirrups, respectively; and z represents the applied axial load ratio (for example, $C8_{1,\ 10\%,\ 8\%,\ 0.2}$). The applied axial loads were 20 and 40% for the specimens numbered from 1 to 5 and 6 to 10, respectively.

Materials

Ready mixed concrete was used for all RC columns, which were placed at the same time. All RC columns were cured for 3 months to avoid changes in the concrete compressive strength after placement. The cylindrical compressive strength of the concrete was obtained on the day of the loading tests. The average cylindrical compressive strength levels of C8, C20, and C30 were 9.47, 27.79, and 37.46 MPa (1373.15, 4029.55, and 5431.70 psi), respectively. The deformed longitudinal reinforcement bars had a diameter of 16 mm (0.63 in.), and yield and rupture strengths of 500 and 590 MPa (72,500 and 85,550 psi), respectively; the corresponding strains were 0.0022 and 0.1156, respectively. After cyclic loading and extraction of the reinforcement bars from the concrete, longitudinal bars were cut into different pieces for each tested RC column, and the mechanical properties of the corroded bars were investigated by conducting tensile tests in accordance with ASTM A370 (2008). In the tests, the cuts were made where the corrosion level was similar to that of uncut bars. As illustrated in Fig. 1, premature yielding and rupturing of the reinforcement bars occurred as the corrosion level increased. It should be emphasized that the effect of corrosion on the stirrups was more pronounced owing to their lower initial mass compared to that of longitudinal bars.

Test specimens

The dimensions and reinforcement details of the RC columns are depicted in Fig. 2. Each tested RC column had a cross section of 300 x 300 mm (11.81 x 11.81 in.) and a length of 2190 mm (86.22 in.) from the footing to the top. The RC columns were reinforced with eight deformed longitudinal reinforcement bars with a diameter of 16 mm (0.63 in.). Deformed stirrups with a diameter of 8 mm (0.31 in.) were used. The intervals of the stirrups were reduced from 150 to 100 mm (5.91 to 3.94 in.) at the

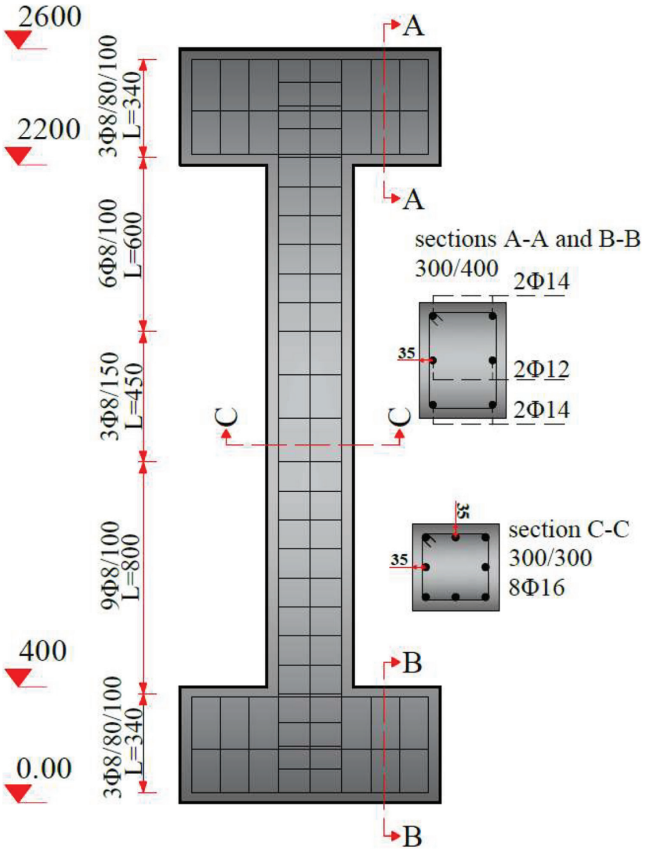


Fig. 2—Section properties.

column densifications to reflect real conditions more accurately. The concrete cover depths used for the RC columns were the same and equal to 35 mm (1.38 in.).

Accelerated corrosion method

The RC columns were subjected to accelerated corrosion after 3 months of curing. Prior to the installation of reinforcing bars and the accelerated corrosion, all reinforcing bars were cleaned by brushing to record their initial mass. A balance with a two-point load cell was used to record the initial mass of each longitudinal bar and stirrup. As illustrated in Fig. 3, once the initial mass of the reinforcement bars was recorded, 4 mm (0.16 in.) diameter stainless copper wires were tied to each longitudinal bar and stirrup prior to placing the concrete. A full-scale accelerated corrosion pool was used for the aging process of the RC columns. Figure 4 depicts a schematic diagram of the accelerated corrosion method. As the corrosion pool was constructed with concrete, plastic membranes were bonded on each surface of the concrete pool to prevent current loss. An adjustable direct current power supply at a rated voltage of 60 V and rated current within the range of 0 to 10 A was used. While the positive outputs of the power supplies were connected to the extended copper wires, which acted as an anode, the stainless copper plates surrounding the RC columns acted as a cathode. The corrosion of reinforcing steel in concrete may be due to internal or external factors. The former includes cement composition, impurities in aggregates, mixing and curing water, water-cement ratio, and admixtures. Internal factors result in the same corrosion level on the inner and

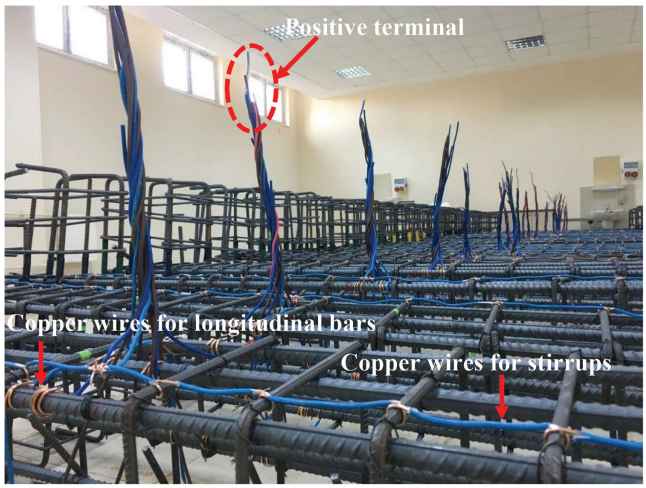


Fig. 3—Copper wires used for reinforcement bars.

outer face of the structural members. Sea salt, which is an external factor, is carried by the wind and may increase the probability of corrosion, particularly on the outer faces of structural members. Yalciner et al. (2015) demonstrated that RC buildings under sea salt attack tend to exhibit higher corrosion levels on the outer face of RC columns compared to the inner face. As illustrated in Fig. 4(b), the water in the corrosion pool was up to the top level of the RC columns, which provided higher corrosion levels for the bottom (that is, positive loading direction). The aim was to reflect the external factors on existing RC buildings, where the outer faces of structural members may be more exposed to corrosion than the inner faces. The corrosion levels were set by considering the degree of degradation owing to corrosion according to the AIJ (1997) guidelines.

Voltmeters were used to estimate the time required for obtaining the desired corrosion level, which was evaluated according to Faraday's law as follows

$$\text{mass loss} = \frac{t(s) \times I(A) \times 55.847}{2 \times 96,487} \quad (1)$$

where t is the time; and I is the current. Faraday's law was used only for monitoring so that the same corrosion level may be attained at three different concrete strength levels. The actual corrosion level (CL) for each RC column was calculated based on Eq. (2)

$$CL = \frac{M_{i-}M_f}{M_i} \times 100 \quad (2)$$

where M_i is the original mass (g) of the reinforcing bars prior to corrosion; and M_f is the final mass (g) of the reinforcement bars following the removal of corrosion products. The total loss in the cross-sectional area (ΔA_s) of the longitudinal bars and the average loss in the cross-sectional area of the stirrups in a column were calculated using Eq. (3)

$$\Delta A_s = A_s \times \frac{\Delta_m}{m} \quad (3)$$

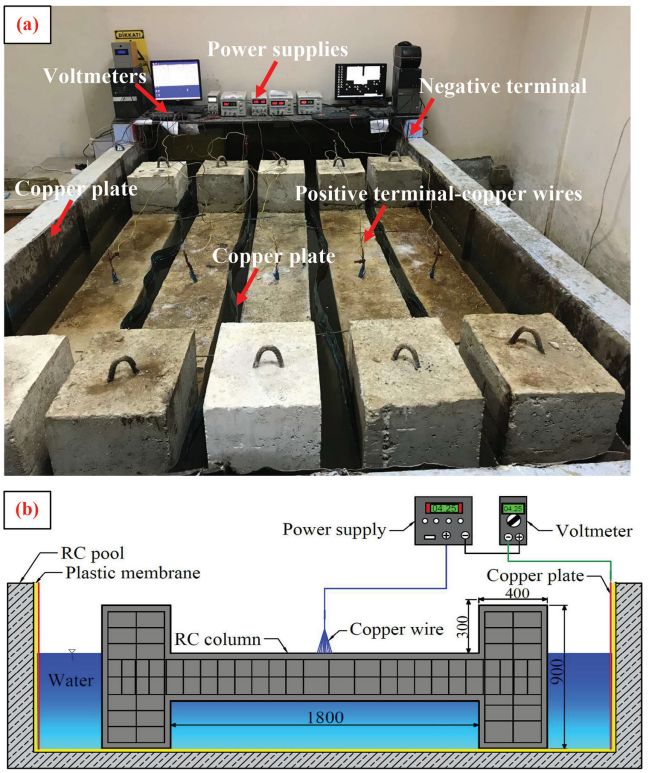


Fig. 4—Accelerated corrosion method: (a) test setup; and (b) schematic diagram.

where A_s is the original cross-sectional area of the reinforcement bars (mm^2); and Δ_m is the mass loss per unit length (g/mm), which was calculated by Eq. (4)

$$\Delta m = m - m' \tag{4}$$

where m and m' are the mass per unit length (g/mm) of the non-corroded and corroded bars, respectively.

The structural behavior resulting from the corrosion acceleration using an impressed direct current technique may be different from that resulting from the corrosion acceleration under an artificial climate environment (Zhang et al. 2009; Grandić and Bjegović 2011; Zhu and François 2014). Yuan et al. (2007) compared the differences in structural behavior under different corrosion techniques. In that study, it was found that the corrosion process and corrosion characteristics of the steel bar under artificial climate environment are similar to that of corrosion under natural environment. Yuan et al. (2007) demonstrated that the failure modes of corroded RC beams were similar at low corrosion levels; however, two different corrosion techniques (that is, impressed direct current technique and artificial climate environment) resulted in different ductility behavior at higher corrosion levels for the same crack width. It has been underlined that the differences in structural behavior under different corrosion techniques are primarily due to different corrosion characteristics on the surface of steel. As observed by Yuan et al. (2007) and Zhu and François (2014), although the galvanostatic method results in more uniform corrosion, the natural corrosion on the surface of the steel bar causes pitting. However, it is also possible to have uniform corrosion (not as uniform as that obtained by using the impressed direct current technique) in reinforcement bars that are corroded in a natural environment. Yalciner et al. (2012a, 2015) demonstrated that the settlement of sea salt (by the wind in marine atmosphere) on the concrete surface may also cause uniform corrosion in steel bars. For the current study, gravimetric tests were conducted on the extracted bars to determine the corrosion levels where pitting corrosion and spatial variability was not considered. Pitting corrosion mainly yields more premature reduction in mechanical properties of steel bars compared to uniform corrosion. Therefore, stirrups compared to longitudinal bars are prematurely ruptured that cause more brittle behavior for RC members due to shear cracking. Previous models were compared in this study based on the impressed direct current technique, and further investigations can be undertaken by considering the effects of corrosion techniques on earthquake indicators.

Loading setup and instrumentation

A schematic diagram of the loading test setup is depicted in Fig. 5. Two axial load ratios (η) of 0.20 and 0.40 were applied, which are defined as the ratio of the applied axial load to the cross-sectional area of an RC column, multiplied by the cylinder compressive strengths ($f_{c\text{-}cylinder}$) of the concrete. Axial loads were applied by means of two hydraulic jacks with a capacity of 1000 kN (225 kip). A hydraulic jack with a capacity of 600 kN (135 kip), which was fixed to the reaction wall, was used for the lateral load. Hinge systems were used for both the vertical and horizontal jacks. The lateral displacements were measured using a linear variable differential transformer (LVDT) placed at the end of the beam at the level of the applied horizontal load. The column footings were firmly mounted with steel plates that were anchored to the floor using 14 steel profiles with a diameter of 16 mm (0.63 in.). Seven strain gauges were bonded on one of the longitudinal bars in the positive loading direction, and one strain gauge in the negative loading direction at the theoretical location of the plastic hinge of the RC columns (that is, 150 mm [5.91 in.] beyond the footing of the column). The bonded strain gauges were used to obtain the yield strength (Q_y) of the RC columns to be used for calculating the damage index.

The loading history followed the standard test procedure for full-scale moment-resistant elements, as defined by FEMA 461 (2007). As illustrated in Fig. 6, three complete cycles using a triangular waveform (that is, loading and unloading) were applied for each drift ratio. RC columns $C30_1$ to $C30_5$ were tested using monotonically increased lateral forces with an axial load ratio of 0.20, which is highly recommended by FEMA 461 (2007), to provide a baseline for the loading history program for cyclic loading and to facilitate the calculation of the damage index.

EXPERIMENTAL RESULTS

Actual corrosion level

All RC columns were broken to extract each longitudinal bar and stirrup from the concrete after the cyclic lateral displacement tests. Chemical cleaning by immersing the reinforcing bars into Clark's solution (HCl) and mechanical cleaning by brushing the reinforcing bars were applied

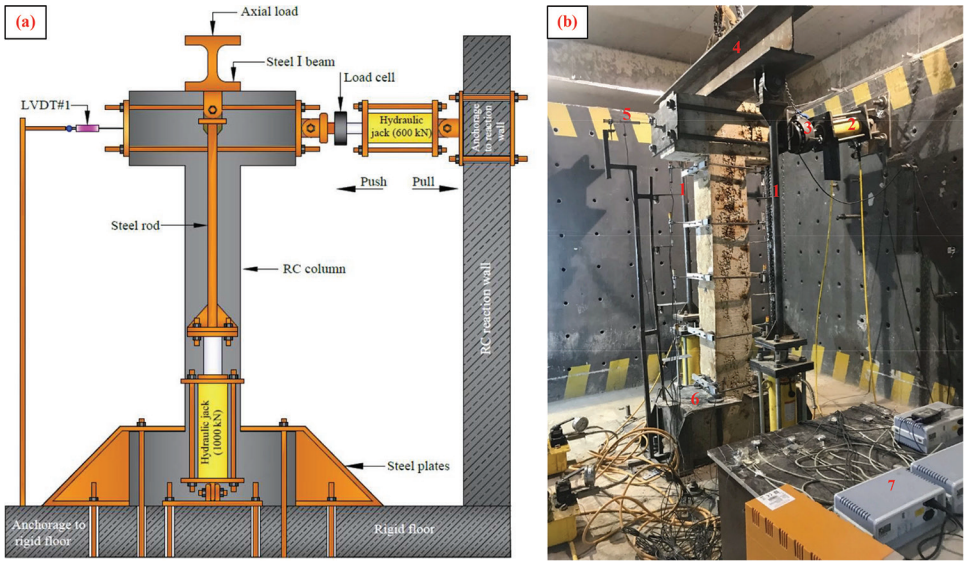


Fig. 5—Test setup for loading: (a) schematic diagram; and (b) photo for test setup.

to remove corrosion products from the reinforcement bar surfaces, according to ASTM G1 (2003). Figure 7 illustrates the applied cleaning process for obtaining the actual corrosion level of the reinforcement bars.

As previous models for corroded RC columns were based on either average or maximum corrosion levels, the detailed gravimetric test results for the reinforcing bars are presented in Table 2. Furthermore, the table presents the average corrosion level of the longitudinal bars (CL_L), average corrosion level in the positive (CL_{Lp}) and negative (CL_{Ln}) loading directions, and average corrosion level of the stirrups (CL_S) using Eq. (2), as well as the corresponding loss in the cross-sectional areas of the reinforcement bars using Eq. (3). As indicated in Table 2, there are significant differences between the obtained actual corrosion levels and the theoretically estimated corrosion levels based on Faraday's law. Specifically, the actual corrosion levels were lower than the theoretical values owing to concrete resistance. Faraday's law considers that the mass loss begins as soon as the current is applied. However, when the steel bars are embedded in concrete, the amount of time and energy are needed until conditions are met for corrosion initiation. An experimental study conducted by Bicer et al. (2018) showed that less than 5% of corrosion levels based on Faraday's law did not allow the corrosion process to begin for large-scale RC beams. As indicated in Table 1, in the study conducted by Meda et al. (2014), the ductility ratio of a corroded RC column increased at a corrosion level of 20%, contradicting the results of other experimental studies. This was due to the overestimation of the corrosion levels by Faraday's law. As indicated in Table 2, the actual corrosion levels at the stirrups were higher compared to the longitudinal bars because of their lower initial mass. Moreover, the average corrosion levels of the longitudinal bars, positive and negative directions, and maximum corrosion levels differed. The effects of the considered corrosion levels (that is, average or maximum corrosion levels) on the seismic behavior of the corroded RC columns for the developed models are explained in the test results.

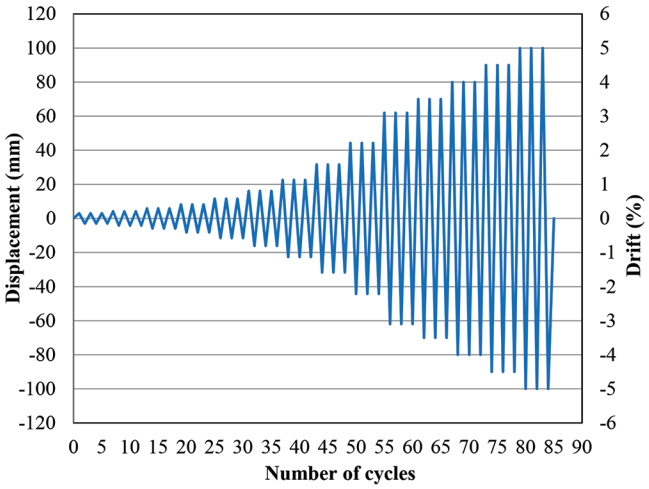


Fig. 6—Loading history program.

Load-displacement results

Owing to the large number of specimens, the selected hysteretic loops of the RC columns are depicted in Fig. 8.

In Fig. 8, differences can be observed between the positive and negative loading directions of the hysteretic loops. The differences between the load-carrying capacities in the two directions were due to the higher corrosion levels in the positive loading direction (that is, the bottom face of the columns in the corrosion pool) of the RC columns, and to non-uniform strength degradation in cyclic loading. The different corrosion levels obtained (that is, asymmetric corrosion levels) in the push and pull directions of the RC columns indicated that as the corrosion levels on the tensile reinforcement bars were higher, the permanent damage also increased when the load was released for initiation of the reversed loading. This was mainly a consequence of stiffness degradation caused by the occurrence of corrosion crack widths during the accelerated corrosion process, which were further opened at the locations of the plastic hinges during loading (for example, refer to Fig. 8(f)). Figure 9 illustrates that as the corrosion level increased and the concrete strength level decreased, the

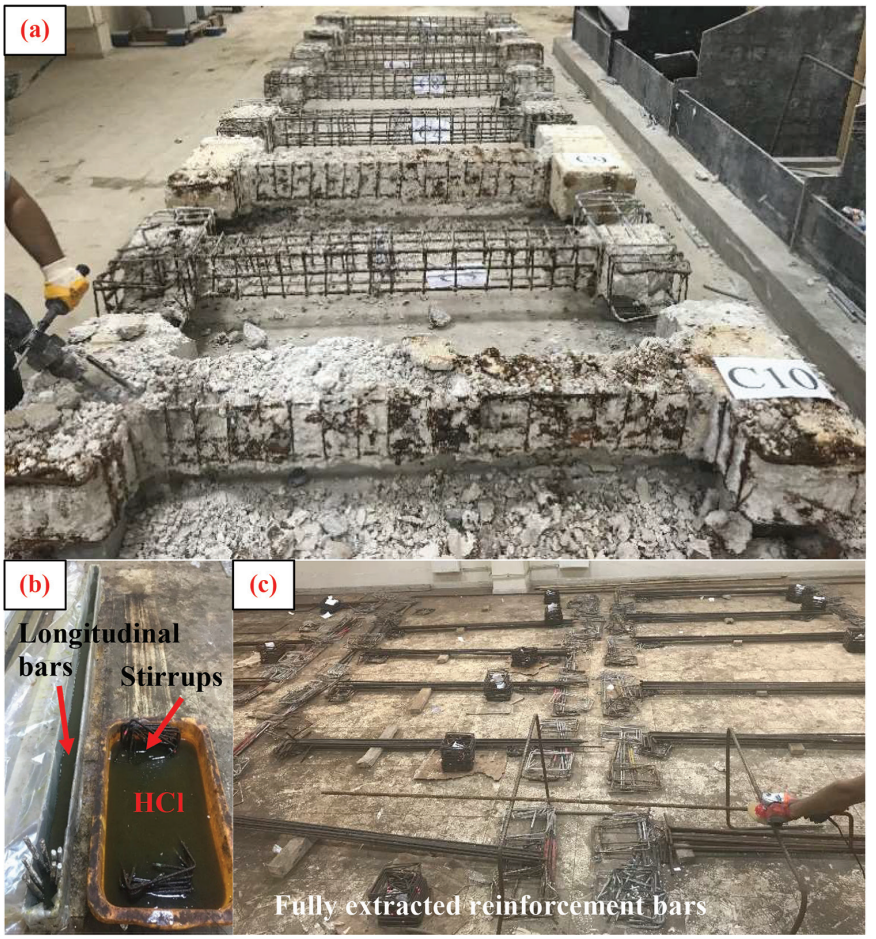


Fig. 7—Process for obtaining actual corrosion levels: (a) breaking of RC columns; (b) chemical cleaning; and (c) mechanical cleaning.

length of the plastic hinges changed as an indicator of the energy dissipation capacity of the tested RC columns.

The yield displacement (Δ_y) and corresponding load (that is, F_y) of all RC columns were calculated according to the procedure described by Sezen and Moehle (2004). The ultimate load (F_u) was defined when the given set of three cycles dropped to 85% of the maximum lateral load. Table 3 summarizes the idealized experimental test results.

According to Fig. 8 and the test results summarized in Table 3, with an axial load ratio of 0.40, the yield strength in the positive loading direction for groups C20 and C30 slightly increased at lower corrosion levels, whereas the yield strength of the C8 specimens exhibited sudden reductions. Similar experimental test results can also be observed in the hysteric curves obtained by Yang et al. (2016) for the increased strength capacity of corroded RC columns. The slight increases in yield strength can be explained by the increased roughness of the steel bars that results from corrosion products filling concrete pores. In Table 3, considering the unilateral (that is, test results discussed for only one loading direction) and bilateral (that is, structural capacity obtained from both loading directions) failure criteria, the yield strength of the corroded RC columns was reduced as corrosion level increased. The reduction percentages of the yield strength for $C8_{10,\ 4.82\%,\ 10.54\%,\ 0.40}$, $C20_{10,\ 5.91\%,\ 10.89\%,\ 0.40}$, and $C30_{10,\ 6.02\%,\ 12.36\%,\ 0.40}$ compared to the non-corroded RC columns were 13.65, 19.67, and 13.98, respectively. Table 3 indicates that the applied axial load ratio dominated the decision-making for the corroded RC columns. When the axial load ratio was reduced to 0.20, the effect of the corrosion level on the structural behavior was not linear, unless bilateral failure criteria were considered. With an axial load ratio of 0.40, slight increases occurred in the ultimate strength capacity in the positive loading directions of groups C20 and C30, whereas the ultimate loads of the C8 specimens exhibited sudden reductions. The reduction in the ultimate load capacity of the severely corroded RC columns $C8_{10}$, $C20_{10}$, and $C30_{10}$ were 17.56, 16.21, and 16.81%, respectively.

The experimental test data (corrosion level and yield and ultimate load of the non-corroded RC columns) from Yang et al. (2016), Li et al. (2018), and the present study were input into the model developed by Ma et al. (2012) to predict the yield and ultimate loads of the corroded RC columns. As the model developed by Ma et al. (2012) was based on unilateral failure criteria, the test results obtained from the unilateral failure criteria were used to predict the experimental tests results. Figure 10 illustrates the ratios of the predicted to experimental values.

It can be observed in Fig. 10 that the model developed by Ma et al. (2012) provided an improved prediction of the yield load of the corroded RC columns compared to the ultimate load for the experimental data obtained by Yang et al. (2016). The lowest

Table 2—Gravimetric test results

Specimen	Sound mass, g		Actual mass loss, g		Achieved actual corrosion level, %		Faraday's corrosion level, %	ΔA_s, mm^2		CL_{Lp}, %	CL_{Ln}, %	CL_{Lpmax}, %	Applied current time-hours ($A.h$)
	L	S	L	S	CL_L	CL_S	$L+S$	ΔA_{sL}	ΔA_{sS}				
$C8_1$	x		0.00	0.00	0.00	0.00	0.00	0.00	0.00	0.00	0.00	0.00	0.00
$C8_2$	32,867.1	8751.0	704.6	363.5	2.14	4.15	6.78	34.48	2.09	2.73	1.74	3.26	2706.5
$C8_3$	32,728.0	8743.5	735.5	418.5	2.25	4.79	8.19	36.15	2.41	2.71	1.85	3.00	3260.5
$C8_4$	32,683.0	8667.5	1580.5	834.0	4.84	9.62	12.18	77.78	4.84	5.92	4.03	6.57	4834.2
$C8_5$	32,836.5	8669.0	1786.0	889.5	5.44	10.26	17.02	87.49	5.16	7.43	3.90	7.90	6781.1
$C8_6$	x		0.00	0.00	0.00	0.00	0.00	0.00	0.00	0.00	0.00	0.00	0.00
$C8_7$	32,771.5	8743.5	937.0	589.5	2.86	6.74	6.51	45.99	3.39	3.68	2.04	4.33	2592.7
$C8_8$	32,799.5	8688.0	1380.0	622.5	4.21	7.17	8.04	67.68	3.60	5.15	3.56	5.74	3200.8
$C8_9$	32,822.5	8649.5	1422.5	783.5	4.33	9.06	12.03	69.71	4.55	5.59	3.16	6.64	4789.3
$C8_{10}$	32,897.0	8667.0	1586.5	913.5	4.82	10.54	17.01	77.57	5.30	7.44	2.62	8.89	6786.8
$C20_1$	x		0.00	0.00	0.00	0.00	0.00	0.00	0.00	0.00	0.00	0.00	0.00
$C20_2$	32,466.0	8127.5	707.0	340.0	2.18	4.18	6.50	35.03	2.10	3.37	1.39	3.61	2533.0
$C20_3$	32,499.0	8038.5	433.5	296.0	1.33	3.68	8.02	21.46	1.85	1.91	0.99	2.29	3121.5
$C20_4$	32,508.5	8024.0	877.0	460.0	2.70	5.73	12.02	43.39	2.88	4.16	1.59	4.87	4674.5
$C20_5$	32,388.5	8007.0	2279.0	922.5	7.04	11.52	17.35	113.18	5.79	10.34	4.09	11.75	6726.6
$C20_6$	x		0.00	0.00	0.00	0.00	0.00	0.00	0.00	0.00	0.00	0.00	0.00
$C20_7$	32,477.0	8023.0	571.0	374.5	1.76	4.67	6.50	28.28	2.35	2.76	1.09	3.56	2526.9
$C20_8$	32,560.0	8063.5	797.5	433.5	2.45	5.38	8.00	39.40	2.70	3.75	1.55	4.26	3118.4
$C20_9$	32,490.0	8098.0	1267.5	680.0	3.90	8.40	12.03	62.75	4.22	5.78	2.33	6.15	4686.1
$C20_{10}$	32,292.0	8078.0	1908.0	880.0	5.91	10.89	16.87	95.04	5.48	9.40	3.22	9.98	6536.4
$C30_1$	x		0.00	0.00	0.00	0.00	0.00	0.00	0.00	0.00	0.00	0.00	0.00
$C30_2$	32,488.5	8124.5	474.5	321.0	1.46	3.95	6.50	23.49	1.99	2.00	0.95	3.63	2533.1
$C30_3$	32,267.5	8099.5	768.5	432.5	2.38	5.34	8.01	38.31	2.68	2.80	1.90	4.60	3104.6
$C30_4$	32,471.5	8012.5	1350.0	683.0	4.16	8.52	12.00	66.87	4.28	5.65	2.86	6.68	4663.9
$C30_5$	32,429.5	8044.5	2064.0	945.5	6.36	11.75	17.00	102.37	5.91	8.52	4.18	10.75	6604.4
$C30_6$	x		0.00	0.00	0.00	0.00	0.00	0.00	0.00	0.00	0.00	0.00	0.00
$C30_7$	32,447.5	8156.5	592.5	330.0	1.83	4.05	6.50	29.37	2.03	2.59	1.09	4.99	2532.3
$C30_8$	32,360.0	7946.5	1028.5	553.5	3.18	6.97	8.00	51.12	3.50	4.56	1.92	5.03	3095.2
$C30_9$	32,447.0	8038.0	1226.0	585.0	3.78	7.28	12.01	60.78	3.66	5.91	1.97	6.79	4666.5
$C30_{10}$	32,447.5	8054.0	1952.0	995.5	6.02	12.36	17.01	96.77	6.21	8.15	4.26	9.79	6613.0

Note: x is non-corroded column; L is total mass of eight longitudinal bars; S is total mass of eighteen stirrups; ΔA_{sL} is total loss in cross-sectional area of longitudinal bars; ΔA_{sS} is average loss in cross-sectional area of stirrups; CL_L is average actual corrosion levels of longitudinal bars; CL_S is average actual corrosion levels at stirrups; CL_{Lp} is average actual corrosion levels of longitudinal bars in positive loading direction; CL_{Ln} is average actual corrosion levels of longitudinal bars in negative loading direction; CL_{Lpmax} is maximum corrosion level in RC column; 1 g = 0.0022 lb; 1 mm^2 = 0.00155 in.^{2}.

calculated ratio was for the ultimate load, and was equal to 0.73 at a corrosion level of 13.25%. The model developed by Ma et al. (2012) overestimated the experimental data obtained by Li et al. (2018). In the study by Li et al. (2018), when the axial load ratio was increased to 0.30 with average corrosion levels of 6.79 and 16.32%, the predicted to experimental yield load ratios were 1.41 and 1.29, respectively. The ratios of the predicted to experimental ultimate load at different corrosion levels with axial loads were also overestimated by Li et al. (2018), and ranged between 1.23 and 1.46. When the present experimental test results were input into the model developed by Ma et al. (2012), it was found that they effectively predicted the yield and ultimate loads of the corroded RC columns. The accurately predicted loads in the current study were at lower corrosion levels compared to those of Ma et al. (2012). In Table 3, the variation coefficients for the ratios of the yield and ultimate loads for the unilateral failure criteria (positive loading direction) to those for the bilateral failure criteria are 0.09 and 0.08, respectively, and were provided to consider the highly corroded positive loading direction for the models of ultimate and yield loads of corroded RC columns. The present data and experimental test data in Ma et al. (2012), Guo et al. (2015), and Li et al. (2018) were used for linear regression analysis to improve the model by Ma et al. (2012), as well as the prediction of the yield (F_{yc}) and ultimate (F_{uc}) loads of the

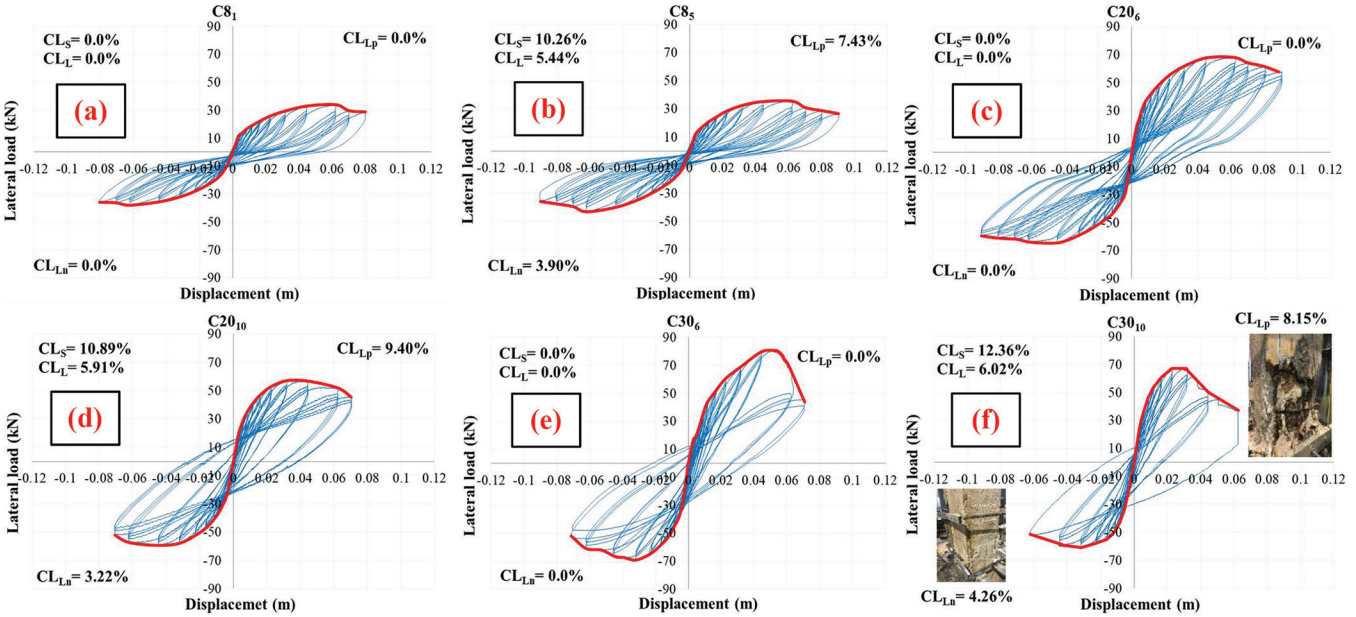


Fig. 8—Hysteretic loops: (a) C8$_1$; (b) C8$_5$; (c) C20$_6$; (d) C20$_{10}$; (e) C30$_6$; and (f) C30$_{10}$.



Fig. 9—Changes in plastic hinge formation of RC columns.

corroded RC columns provided by Eq. (5) and (6). The newly developed models effectively captured the previous experimental results by considering the present study. The correlation coefficients in Eq. (5) and (6) are 0.90 and 0.87, respectively, and the corresponding root mean square of the error estimates are 0.037 and 0.039.

$$F_{yc} = F_{yo}\left(\frac{1}{1+0.039\times CL_L}\right) \quad (5)$$

$$F_{uc} = F_{uo}\left(\frac{1}{1+0.033\times CL_L}\right) \quad (6)$$

Table 3—Experimental test results

Specimen	Positive loading direction					Negative loading direction					Bilateral failure criteria					
	F_y, kN (kip)	F_u, kN (kip)	Δ_y, m (in.)	Δ_u, m (in.)	μ_D	F_y, kN (kip)	F_u, kN (kip)	Δ_y, m (in.)	Δ_u, m (in.)	μ_D	F_y, kN (kip)	F_u, kN (kip)	μ_D	μ_E	E (kN.m)	η
$C8_1$	27.49 (6.19)	28.68 (6.45)	0.03 (1.12)	0.08 (3.15)	2.82	30.47 (6.86)	35.91 (8.08)	0.03 (1.13)	0.08 (3.17)	2.80	28.98 (6.52)	32.30 (7.27)	2.81	3.67	11.94	0.20
$C8_2$	34.93 (7.86)	36.87 (8.30)	0.03 (1.03)	0.09 (3.45)	3.35	33.54 (7.55)	35.13 (7.90)	0.03 (1.06)	0.09 (3.67)	3.45	34.24 (7.70)	36.00 (8.10)	3.40	4.15	13.91	0.20
$C8_3$	29.41 (6.62)	31.36 (7.06)	0.02 (0.76)	0.06 (2.50)	3.31	26.76 (6.02)	28.84 (6.49)	0.02 (0.78)	0.06 (2.50)	3.22	28.09 (6.32)	30.10 (6.77)	3.26	5.63	12.67	0.20
$C8_4$	23.91 (5.38)	24.27 (5.46)	0.02 (0.69)	0.06 (2.49)	3.63	17.83 (4.01)	19.40 (4.37)	0.02 (0.75)	0.03 (1.34)	1.79	20.87 (4.70)	21.84 (4.91)	2.71	5.55	11.25	0.20
$C8_5$	28.78 (6.48)	30.10 (6.77)	0.03 (1.00)	0.07 (2.86)	2.86	35.19 (7.92)	36.73 (8.26)	0.04 (1.39)	0.08 (3.29)	2.37	31.99 (7.20)	33.42 (7.52)	2.61	3.36	10.88	0.20
$C8_6$	33.12 (7.45)	35.99 (8.10)	0.03 (1.02)	0.10 (3.85)	3.79	26.79 (6.03)	28.58 (6.43)	0.02 (0.88)	0.10 (3.85)	4.39	29.96 (6.74)	32.29 (7.26)	4.09	7.60	23.31	0.40
$C8_7$	30.22 (6.80)	33.13 (7.45)	0.02 (0.89)	0.09 (3.60)	4.05	29.69 (6.68)	32.16 (7.24)	0.02 (0.78)	0.10 (3.93)	5.04	29.96 (6.74)	32.65 (7.35)	4.54	9.73	24.52	0.40
$C8_8$	21.00 (4.73)	27.95 (6.29)	0.02 (0.89)	0.10 (3.98)	4.47	35.15 (7.91)	37.21 (8.37)	0.02 (0.98)	0.10 (3.94)	4.03	28.08 (6.32)	32.58 (7.33)	4.25	6.72	24.33	0.40
$C8_9$	30.40 (6.84)	32.44 (7.30)	0.02 (0.86)	0.09 (3.56)	4.17	28.89 (6.50)	30.21 (6.80)	0.02 (0.89)	0.09 (3.55)	3.98	29.65 (6.67)	31.33 (7.05)	4.07	5.35	22.16	0.40
$C8_{10}$	28.60 (6.44)	29.67 (6.68)	0.02 (0.84)	0.06 (2.45)	2.92	27.42 (6.17)	30.13 (6.78)	0.02 (0.75)	0.07 (2.77)	3.69	28.01 (6.30)	29.90 (6.73)	3.31	4.95	13.81	0.40
$C20_1$	51.71 (11.63)	53.68 (12.08)	0.03 (1.18)	0.11 (4.19)	3.54	45.14 (10.16)	47.57 (10.70)	0.02 (0.90)	0.06 (2.39)	2.67	48.43 (10.90)	50.63 (11.39)	3.11	6.09	29.53	0.20
$C20_2$	49.10 (11.05)	48.53 (10.92)	0.03 (1.17)	0.10 (3.75)	3.21	47.55 (10.70)	51.05 (11.49)	0.04 (1.57)	0.07 (2.93)	1.86	48.33 (10.87)	49.79 (11.20)	2.54	5.54	28.70	0.20
$C20_3$	59.64 (13.42)	59.45 (13.38)	0.03 (1.24)	0.10 (3.94)	3.17	38.10 (8.57)	40.42 (9.09)	0.02 (0.83)	0.05 (2.12)	2.55	48.87 (11.00)	49.94 (11.24)	2.86	7.01	29.98	0.20
$C20_4$	49.95 (11.24)	53.74 (12.09)	0.02 (0.91)	0.08 (3.16)	3.46	43.91 (9.88)	46.56 (10.48)	0.03 (1.02)	0.08 (3.17)	3.10	46.93 (10.56)	50.15 (11.28)	3.28	7.50	32.03	0.20
$C20_5$	53.85 (12.12)	55.62 (12.51)	0.02 (0.76)	0.08 (3.21)	4.22	39.01 (8.78)	41.42 (9.32)	0.02 (0.93)	0.09 (3.57)	3.84	46.43 (10.45)	48.52 (10.92)	4.03	9.44	36.30	0.20
$C20_6$	54.91 (12.35)	57.82 (13.01)	0.02 (0.90)	0.09 (3.48)	3.88	50.00 (11.25)	59.62 (13.41)	0.02 (0.76)	0.09 (3.56)	4.70	52.46 (11.80)	58.72 (13.21)	4.29	9.85	45.79	0.40
$C20_7$	59.72 (13.44)	61.37 (13.81)	0.02 (0.96)	0.08 (3.12)	3.24	48.11 (10.82)	54.88 (12.35)	0.02 (0.72)	0.09 (3.47)	4.83	53.92 (12.13)	58.13 (13.08)	4.04	8.19	39.45	0.40
$C20_8$	55.98 (12.60)	59.02 (13.28)	0.02 (0.85)	0.07 (2.71)	3.20	47.13 (10.60)	55.22 (12.42)	0.02 (0.66)	0.08 (3.14)	4.75	51.56 (11.60)	57.12 (12.85)	3.97	7.82	35.49	0.40
$C20_9$	51.48 (11.58)	52.46 (11.80)	0.02 (0.64)	0.06 (2.45)	3.85	46.34 (10.43)	50.71 (11.41)	0.02 (0.79)	0.07 (2.78)	3.53	48.91 (11.00)	51.59 (11.61)	3.69	5.43	19.74	0.40
$C20_{10}$	44.11 (9.92)	48.45 (10.90)	0.02 (0.68)	0.06 (2.45)	3.62	47.27 (10.64)	52.05 (11.71)	0.02 (0.77)	0.07 (2.78)	3.62	45.69 (10.28)	50.25 (11.31)	3.62	5.25	18.52	0.40
$C30_1$	42.10 (9.47)	42.71 (9.61)	0.04 (1.48)	0.13 (4.93)	3.32	M	M	M	M	M	M	M	M	M	5.24	0.20
$C30_2$	44.05 (9.91)	44.19 (9.94)	0.02 (0.69)	0.04 (1.47)	2.14	M	M	M	M	M	M	M	M	M	1.47	0.20
$C30_3$	46.14 (10.38)	59.65 (13.42)	0.01 (0.34)	0.02 (0.98)	2.88	M	M	M	M	M	M	M	M	M	1.22	0.20
$C30_4$	42.61 (9.59)	49.06 (11.04)	0.03 (1.30)	0.07 (2.58)	1.98	M	M	M	M	M	M	M	M	M	2.51	0.20
$C30_5$	42.03 (9.46)	50.31 (11.32)	0.03 (1.16)	0.05 (1.95)	1.67	M	M	M	M	M	M	M	M	M	1.75	0.20

Table 3 (cont.)—Experimental test results

Specimen	Positive loading direction					Negative loading direction					Bilateral failure criteria					
	F_y, kN (kip)	F_u, kN (kip)	Δ_y, m (in.)	Δ_u, m (in.)	μ_D	F_y, kN (kip)	F_u, kN (kip)	Δ_y, m (in.)	Δ_u, m (in.)	μ_D	F_y, kN (kip)	F_u, kN (kip)	μ_D	μ_E	E (kN.m)	ɳ
$C30_6$	64.83 (14.59)	68.54 (15.42)	0.03 (1.08)	0.07 (2.61)	2.41	55.35 (12.45)	58.82 (13.23)	0.01 (0.54)	0.07 (2.65)	4.87	60.09 (13.52)	63.68 (14.33)	3.64	8.43	22.09	0.40
$C30_7$	65.65 (14.77)	69.66 (15.67)	0.02 (0.72)	0.05 (2.01)	2.79	45.99 (10.35)	50.33 (11.32)	0.01 (0.53)	0.06 (2.38)	4.49	55.82 (12.56)	60.00 (13.50)	3.64	8.52	22.46	0.40
$C30_8$	67.40 (15.17)	67.97 (15.29)	0.02 (0.78)	0.05 (1.78)	2.29	48.66 (10.95)	51.68 (11.63)	0.01 (0.49)	0.06 (2.34)	4.81	58.03 (13.06)	59.83 (13.46)	3.55	7.45	19.20	0.40
$C30_9$	55.34 (12.45)	56.68 (12.75)	0.01 (0.57)	0.03 (1.32)	2.31	51.89 (11.68)	57.17 (12.86)	0.01 (0.46)	0.04 (1.73)	3.77	53.62 (12.06)	56.93 (12.81)	3.04	5.75	14.51	0.40
$C30_{10}$	55.77 (12.55)	57.02 (12.83)	0.01 (0.57)	0.04 (1.49)	2.61	50.26 (11.31)	53.65 (12.07)	0.01 (0.54)	0.04 (1.70)	3.16	53.02 (11.93)	55.34 (12.45)	2.89	5.60	12.14	0.40

Note: E is cumulative energy dissipation capacity at 85% of ultimate load; M is monotonic loading.

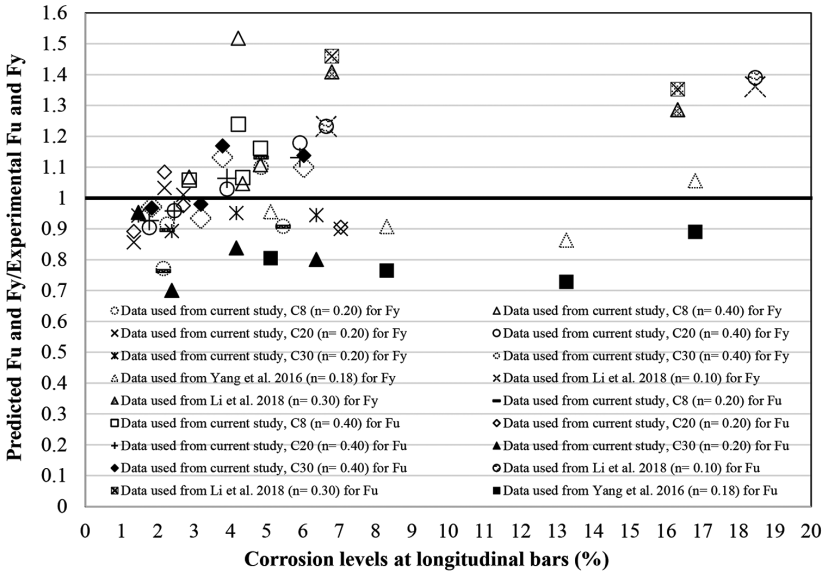


Fig. 10—Ratios of predicted to experimental values using Ma et al. (2012).

Displacement ductility

The displacement ductility ratio ($\mu_D = \Delta_u/\Delta_y$) of each RC column was calculated by dividing the ultimate displacement by the yield displacement. According to the summarized test results in Table 3, the bilateral and unilateral failure criteria exhibited significant differences in terms of the ductility ratio of the corroded RC columns. At different corrosion and concrete strength levels, the displacement ductility ratios were different for positive and negative loading directions. In Table 3, increased ductility ratios of the corroded RC columns for the unilateral failure criteria are considered. The increase in the ductility ratio of the corroded RC columns was also investigated in the study by Li et al. (2018). In the present study, the increase in the ductility ratio was more obvious for the C8 RC columns with an axial load ratio of 0.20. This was due to the lower impact of the axial load ratio, with a greater confinement effect of corrosion products at lower concrete strength levels. The increased ductility ratio at lower corrosion levels can be partially explained by the confinement provided by corrosion products (that is, the effect of corrosion on bond-slip relationships). The study by Yalciner et al. (2012b), where pullout tests were conducted on corroded concrete specimens, and the flexural strength of corroded RC beams (Yalciner et al. 2018) also emphasized this phenomenon. In the study by Yalciner et al. (2012b), it was concluded that the bond strength degradation at higher concrete strength levels occurred at lower corrosion levels. Another cause of the increased ductility ratio was the premature yielding of the corroded reinforcement bars. In addition, the affected mechanical properties of the reinforcing bars and concrete spalling owing to volumetric expansion by the corrosion products reduced the yield load of the corroded RC columns. When bilateral failure criteria were considered, the test results, as presented in Table 3, indicated that the ductility ratio of the corroded RC columns increased for lower corrosion levels, and then decreased with increased corrosion levels (as was expected from the structural behavior of the corroded RC members). Considering the bilateral failure criteria, the reduction in the ductility ratio of the highly corroded RC columns $C8_{10,\ 4.82\%,\ 10.54\%,\ 0.40}$, $C20_{10,\ 5.91\%,\ 10.89\%,\ 0.40}$, and $C30_{10,\ 6.02\%,\ 12.36\%,\ 0.40}$ was 19.23%, 15.62%, and 20.61%, respectively.

The two models developed by Ma et al. (2012) and Yang et al. (2016) were used to predict the displacement ductility

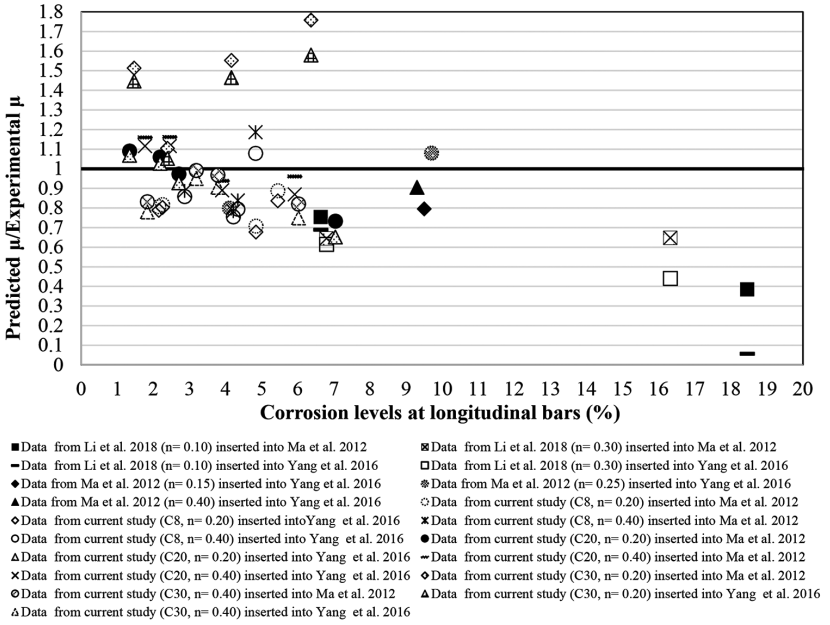


Fig. 11—Ratios of predicted to experimental values using Ma et al. (2012) and Yang et al. (2016).

ratio of the corroded RC columns in the present study and in experimental data obtained in Li et al. (2018). Figure 11 depicts the ratios of the predicted to experimental values. As the models were based on unilateral failure criteria, the obtained test results (that is, the positive loading direction) were used to predict the experimental results.

In Fig. 11, by considering the two models, the calculated lowest values for the descending branches of the displacement ductility ratio for C8, C20, and C30 were 0.68, 0.73, and 0.75, respectively. In Fig. 11, the improved prediction by Ma et al. (2012) compared to that by Yang et al. (2016) was due to the considered average corrosion levels of the longitudinal bars under cyclic loading. The model developed by Ma et al. (2012) considered the average corrosion level of the longitudinal bars to predict the displacement ductility ratio, whereas Yang et al. (2016) considered the maximum corrosion level of the longitudinal bars. It is well known the ductility behavior of RC members depends on the confinement effect by the stirrups. As indicated in Table 2, there is a strong relationship between the average corrosion levels of the longitudinal bars and the stirrups. The variation coefficient for the ratio of the corrosion level of the stirrups to that of the longitudinal bars was 0.18. Therefore, to reflect the effect of the stirrups on the ductility ratio of the corroded RC columns, the considered average corrosion level of the longitudinal bars provided superior predictions of structural indicators for corroded RC columns. The models developed by Ma et al. (2012) and Yang et al. (2016) underestimated the ductility ratio of the corroded RC columns for the study by Li et al. (2018). It can be observed from Fig. 11 that the ratio of the predicted to experimental values using the approach by Ma et al. (2012) varied from 0.39 to 0.75. When the corrosion levels obtained by Li et al. (2018) were input into the model by Yang et al. (2016), the resulting ductility ratio varied from 0.06 to 0.69.

It should be noted that the experimentally obtained displacement ductility ratio of all corroded RC columns were increased in the study by Li et al. (2018). In contrast to the results of Yang et al. (2016), the experimentally obtained ductility ratio of a column in the study by Ma et al. (2012) also increased by 15% at a corrosion level of 4.1%. The increase in the ductility ratio of a corroded RC column in another study by Guo et al. (2015) was 4% at a corrosion level of 5.07%. Although the experimentally obtained ductility ratios in Ma et al. (2012) were increased for certain corrosion levels, the model by Ma et al. (2012) considered that the ductility ratios were reduced for each given corrosion level. When the experimental results in Ma et al. (2012) were revisited, it was found that the significantly decreased ductility ratios were due to not only to the increased corrosion levels but also the increased axial loads, for which the increased axial load ratios (0.60, 0.75, and 0.90) of the corroded RC columns were not tested for comparison with non-corroded columns. The contradicting results for the displacement ductility ratio of the corroded RC columns were due to the considered unilateral failure criteria, as well as the increased ductility ratios determined by the displacement-based method (that is, $\mu_D = \Delta_u/\Delta_y$). As indicated in Table 3, the determined ductility ratio of a corroded RC column was increased for a positive loading direction, whereas the ductility ratio was reduced for a negative direction, and differences were evident among the other specimens. This was due to the non-uniform strength degradation of RC columns under cyclic loading with dissipated energy capacity, which becomes more evident with asymmetric corrosion levels. Even in the absence of corrosion, cyclic loading may cause non-uniform strength degradation (Ma et al. 2012; Li et al. 2018). Therefore, it is conceivable that under cyclic loading of corroded RC columns, bilateral failure criteria yield superior results in terms of displacement ductility ratio. Moreover, the authors of this paper agreed with the increase in the ductility ratio of corroded RC columns up to a certain corrosion level, as indicated by Li et al. (2018), and identified further experimental data in

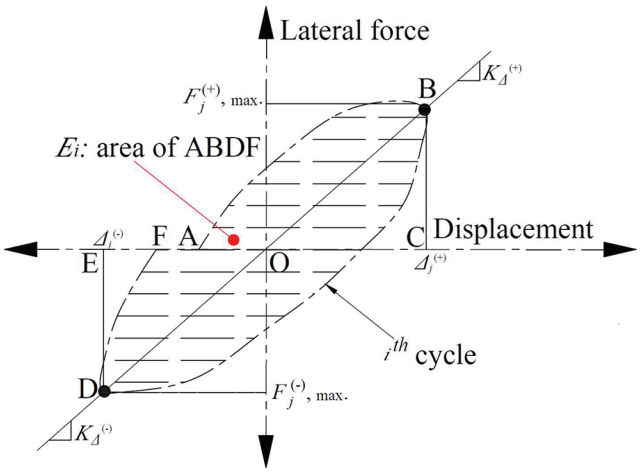


Fig. 12—Schematic for energy dissipation.

other studies (Ma et al. 2012; Guo et al. 2015). However, it is also believed that it is not easy to define a corrosion level limit state precisely for the ascending and descending branches of the ductility ratio of corroded members, owing to the numerous corrosion-related parameters. It is clear that as the corroded reinforcement bars yielded prematurely compared to the non-corroded bars, the ductility ratios calculated according to the displacement-based method considering unilateral failure criteria were misleading in terms of the structural behavior of corroded RC columns, despite the fact that corroded RC columns absorb less energy prior to failure. Therefore, the authors of this paper suggest calculating the energy-based ductility index (that is, $\mu_E = E/E_y$) in the case of corrosion, by dividing the cumulative energy dissipation by the cumulative dissipated energy at yield strength. As indicated in Table 3, the determined ductility index of the corroded RC columns (that is, μ = 0.40) according to the energy-based method was reduced as corrosion level increased, further demonstrating the effects of corrosion. A new model was developed to predict the displacement ductility ratio of the corroded RC columns by considering the energy-based displacement ductility index, as per Eq. (7). The coefficient of correlation in Eq. (7) was 0.78 having a root mean square of error estimate of 0.079.

$$\mu_c = \mu_o(0.91^{CL_L}) \quad (7)$$

Energy dissipation capacity

The cumulative energy dissipation capacity of all RC columns was calculated using Eq. (8) and Fig. 12, and the test results are summarized in Table 3

$$E = \sum_{i=1}^{n} E_i \quad (8)$$

where E is the sum of all hysteretic loops; and E_i is calculated from the energy dissipated at each positive and negative cyclic loop. In Eq. (8), the total dissipated energy of the tested RC columns was determined by the sum of all loading cycles until the lateral force of the member was reduced to 85% of the maximum load.

The previously noted effects of lower axial load ratio on earthquake indicators were also valid for the energy dissipation capacity of the corroded RC columns. It can be observed in Table 3 that when the axial load ratio was 0.20, the reduction in the energy dissipation capacity was not significant compared to the value of 0.40. The reduction in the energy dissipation capacity of the severely corroded RC columns $C8_{10,\ 4.82\%,\ 10.54\%,\ 0.40}$, $C20_{10,\ 5.91\%,\ 10.89\%,\ 0.40}$, and $C30_{10,\ 6.02\%,\ 12.36\%,\ 0.40}$ was 40.77%, 59.55%, and 45.03%, respectively. Contradictions were found in terms of the energy dissipation of corroded RC columns in the literature. Ma et al. (2012) (increased up to 14% of the corrosion level and then decreased) and Meda et al. (2014) (increased up to 20% of the corrosion level) noticed that the energy dissipated by the corroded columns was higher than that of the non-corroded columns, while Guo et al. (2015), Yang et al. (2016), Liu et al. (2017), and Yuan et al. (2017) observed a decrease in the energy dissipation of corroded RC columns. This contradiction also confirms the previously noted challenges regarding the ductility ratio. The expected large amount of inelastic energy dissipated at the plastic hinges may be reflected by large inelastic deformations with increased ductility ratio. Therefore, the models developed for the prediction of the displacement ductility ratio of corroded RC columns should be related to energy dissipation capacity. As indicated in Table 3, the progressive reduction in energy dissipation capacity refers to the energy-based method, as proposed in the present study, so that the developed model may predict the ductility ratio of corroded RC columns under cyclic loading.

Experimental test data from Ma et al. (2012), Guo et al. (2015), and the present study were input into the model by Yang et al. (2016) to predict the experimentally obtained energy dissipation of corroded RC columns. As the exact corrosion levels at all reinforcement bars were not available in these experimental studies, the average corrosion levels provided were input into the model by Yang et al. (2016). Figure 13 depicts the ratios of the predicted to experimental values.

The model by Yang et al. (2016), illustrated in Fig. 13, was based on the same applied axial load ratio of 0.18, for which the model effectively predicted the experimentally obtained values by Ma et al. (2012) up to an axial load ratio of 0.25, but for lower corrosion levels. At higher corrosion levels with increased axial loads, the ratio of the predicted to experimental values for Ma et al. (2012) was 1.56 and 1.67. It was found that that model developed by Yang et al. (2016) is safe if the axial load ratio is high and the corrosion level is low, or the corrosion level is low and the axial load is high, owing to the unique axial load ratio used in their experimental program. The effectively predicted experimental data in the study by Guo et al. (2015) also supported this finding. In Fig. 13, it can be observed that the model developed by Yang et al. (2016) accurately predicted the experimentally obtained dissipated energy in Guo et al. (2015). The accurately predicted experimental data in Guo et al. (2015) were provided by similar applied axial load ratios (that is, 0.10 to 0.18) and concrete strength levels. When the current experimental test results were input into the model by Yang et al. (2016), using the 46.4 MPa (6728 psi) cubic concrete strength level of Yang et al. (2016), the dissipation energy of the corroded RC columns for group C30 was reasonably well predicted ($f_{c\text{-}cubic}$ = 46.8 MPa [6786 psi]). In

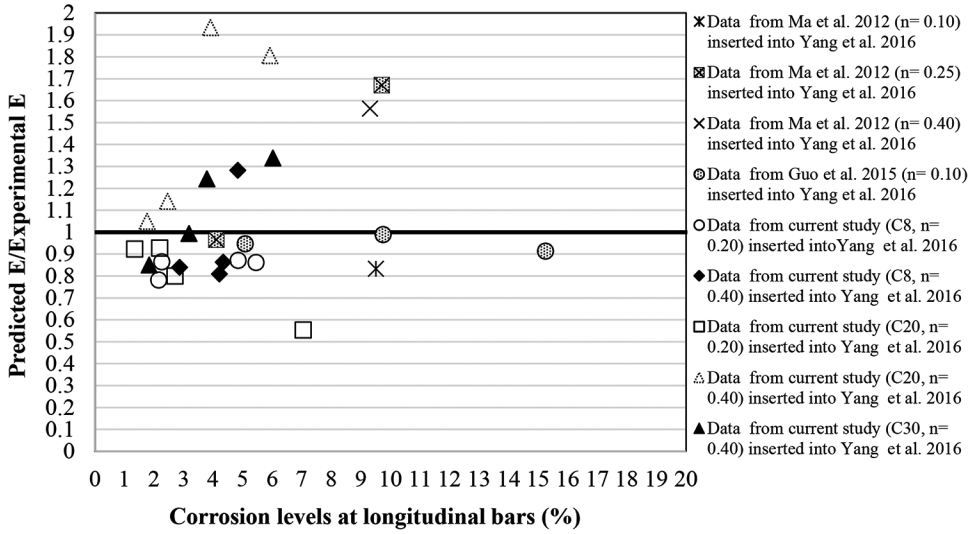


Fig. 13—Ratio of predicted energy dissipation capacities using Yang et al. (2016).

Fig. 13, it can be observed that the predicted energy dissipation capacity ratio for C30 ranged between 0.85 and 1.34. Although the maximum corrosion levels of the current study were within the corrosion level limits obtained by Yang et al. (2016), owing to the corrosion effects on the concrete strength levels, the calculated lowest ratio for C20 ($f_{c\text{-}cubic}$ = 34.7 MPa [5423 psi]) was 1.93. The present experimental test results re-emphasize the corrosion effects on concrete strength levels in terms of corrosion crack widths owing to volumetric expansion by corrosion products (which also relates to Fig. 9) indicating the changes in the plastic hinge formation of RC columns.

The present experimental test results demonstrated that the energy dissipation capacity was a major and significant effect of corrosion for different concrete strength levels. When the permeability of a lower concrete strength level is considered, the corrosion and seismic risks are higher for older RC buildings. A study by Cağatay (2005) investigated the effects of concrete quality on building collapses during the June 27, 1998 Adana-Ceyhan and the August 17, 1999 Izmit earthquakes in Turkey. It was determined that most collapsed buildings were constructed with concrete strength levels lower than 10 MPa (1450 psi), and unwashed sea sands with seashells were found in the concrete of these collapsed buildings. A study conducted by Shimizu et al. (2000) also emphasized the existence of lower concrete strength (less than 13 and 10 MPa [1885 and 1450 psi]) in Japan for RC buildings constructed between 1926 and the 1980s. Therefore, it is important to predict the energy dissipation capacity of lower concrete strength levels, considering the available literature. Owing to the greater confinement provided by corrosion products at C8, two different empirical models were developed to predict the energy dissipation capacities of lower and higher concrete strength levels, as expressed by the following equations

$$\frac{E_c}{E_o} = 1 + 0.34 \times CL_L - 0.19CL_L^{1.5} \text{ for C8} \quad (9)$$

$$\frac{E_c}{E_o} = \frac{1}{1 + 0.024 \times CL_L + 0.035CL_L^2} \text{ for C20 to 30} \quad (10)$$

The coefficients of correlation were 0.97 and 0.99 in Eq. (9) and (10), with root mean square of error estimates of 0.039 and 0.021, respectively.

Stiffness degradation

The stiffness of each RC column was calculated by the following equations, according to Sun et al. (2008)

$$K_\Delta = \frac{K_\Delta^+ + K_\Delta^-}{2} \quad (11)$$

$$K_\Delta^+ = \sum_{j=1}^{3} F_{j,max}^+ / \sum_{j=1}^{3} \Delta_j^+, \; K_\Delta^- = \sum_{j=1}^{3} F_{j,max}^- / \sum_{j=1}^{3} \Delta_j^- \quad (12)$$

where $F_{j,max}$ and Δ_j are the maximum lateral load within a cycle and its corresponding displacement, respectively (refer to Fig. 12). The calculated stiffness for each displacement was normalized with respect to the stiffness of the first three cycles, as illustrated in Fig. 14.

In Fig. 14, it can be observed that there was strong agreement of the initial stiffness of the corroded RC columns in the available literature (Ma et al. 2012; Meda et al. 2014; Di Carlo et al. 2017; Liu et al. 2017), where the corrosion in the reinforcement bars had an insignificant effect on the initial stiffness degradation. The average normalized secant stiffness (K_s) of each group of RC columns was determined according to the procedure described by Ma et al. (2012). The ratio of the average normalized secant stiffness of the corroded columns (K_{sc}) to the non-corroded columns (K_{so}) is indicated in Fig. 15.

As illustrated in Fig. 15, as the corrosion level increased, the secant stiffness of the corroded RC columns decreased progressively, owing primarily to the wider opened cover cracking of the concrete. With an axial load ratio of 0.40, the percentage reduction in the secant stiffness of severely corroded RC columns $C8_{10}$ and $C30_{10}$ was greater than that of $C20_{10}$, at 34%. The reason for the additional degradation in secant stiffness of C8 and C30 was the lower strength capacity of C8 and the effect of corrosion products at higher concrete strength levels, whereby the concrete became more brittle compared to lower strength concrete

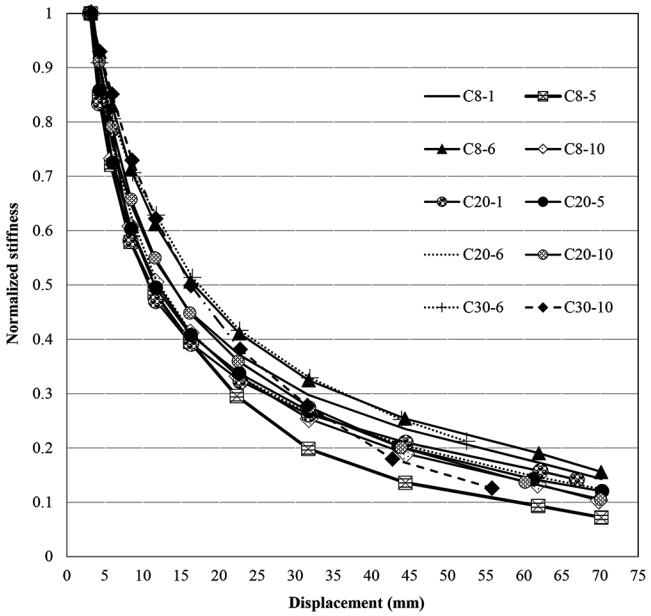


Fig. 14—Normalized stiffness degradation.

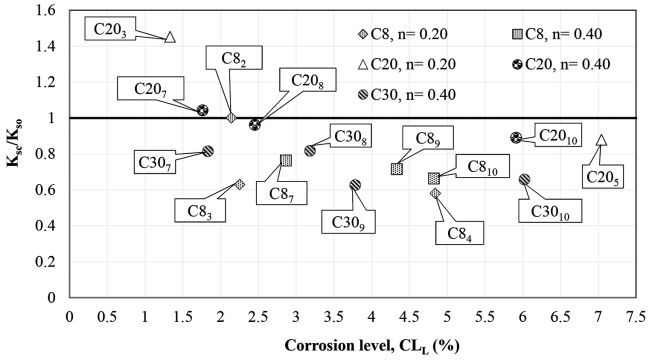


Fig. 15—Average secant stiffness.

levels, as investigated in an early study by Yalciner et al. (2012b). In Fig. 15, the reduction in secant stiffness of $C20_5$ was 12%, whereas it was 42% at $C8_4$ with an applied axial load ratio of 0.20. This provided evidence that the corrosion effects differed at varying concrete strength levels. The model developed by Ma et al. (2012) using the 32.4 MPa (469 psi) concrete strength level effectively predicted the average normalized secant stiffness of C20 ($f_{c\text{-}cubic}$ = 34.7 MPa [5423 psi]), and overestimated C8 and C30, which supports the previous finding of greater degradation in the secant stiffness of C8 and C30. The model developed by Ma et al. (2012) is suggested for use in further studies for the prediction of the normalized secant stiffness of C20. Equation (13) was developed to predict the ratio of the average normalized secant stiffness of corroded RC columns (K_{sc}) to non-corroded columns for C8 and C30, where the correlation coefficient was 0.84, with a root mean square of error estimate of 0.065.

$$\frac{K_{sc}}{K_{so}} = \left(1 + CL_L\right)^{-0.24} \tag{13}$$

Damage index

It is important to conclude the seismic behavior of corroded RC columns in terms of damage level. The model developed by Park and Ang (1985) was used to calculate the damage state of the RC columns according to the following equation

$$D_i = \frac{\delta_m}{\delta_u} + \frac{\beta}{Q_y \delta_u} \int dE \tag{14}$$

where δ_m and δ_u are the maximum and ultimate deformations under seismic and monotonic loads, respectively; Q_y is the yield strength when the steel bar yields; dE is the incremental adsorbed hysteretic energy; and β is a model parameter representing the effect of cyclic loading on the structural damage, which was taken as 0.05 according to Park et al. (1987). The quantities δ_m, Q_y, and dE were adopted from the present experimental data. The experimentally obtained relationships among the monotonically loaded RC columns $C30_1$ to $C30_5$ and cyclic loaded columns $C30_5$ to $C30_{10}$ were used to predict the ultimate deformations of C8 and C20 under monotonic loads. As indicated in Table 3, there was a strong relationship between the ultimate loads of $C30_1$ to $_5$ (monotonically loaded) and $C30_5$ to $_{10}$ (cyclic loaded). The ratio of the ultimate loads of the monotonically loaded RC columns to the cyclic loaded RC columns were 0.62 and 0.63 for the non-corroded ($C30_1/C30_6$) and the least corroded RC columns ($C30_2/C30_7$), respectively. These ratios were 0.88, 0.87, and 0.88, respectively, for further corrosion levels ($C30_{3\ldots5}$/ $C30_{8\ldots10}$). The determined ratios were used for the prediction of the ultimate deformations under monotonically loaded RC columns at C8 and C20. Figure 16 depicts the determined damage index of the RC columns corresponding to drift ratios. The associated performance levels (immediate occupancy, operational, life safety, and collapse prevention) corresponding to roof drift ratios are illustrated in Fig. 16 according to Vision 2000 (1995). The definitions of the damage index of conventional RC buildings were also defined based on Varum (2003) in the same figure.

As illustrated in Fig. 16, the damage index of the non-corroded RC columns increased as the concrete strength level was reduced. In the case of corrosion, the damage index of the corroded RC columns increased as corrosion level increased and the concrete strength level was reduced. The determined damage index of the severely corroded RC column $C30_{10}$ was 0.62, corresponding to the associated performance level of immediate occupancy (0.2% of the drift ratio), whereas the damage index of $C8_{10}$ and $C20_{10}$ was 0.91 and 0.87, respectively. According to Vision 2000 (1995), repair is possible for conventional structures when the drift ratio is less than 1.5% (that is, a limit state of life safety). However, as illustrated in Fig. 16, the determined damage index of $C8_{10}$ and $C20_{10}$ was greater than 1 when the drift ratio was 1.5%. Therefore, it is evident from Fig. 16 that the seismic performance level of the RC columns was significantly affected by corrosion, which requires the limit states of the performance level of corroded RC columns to be redefined for decision making on the repair and strengthening of such structures in further studies.

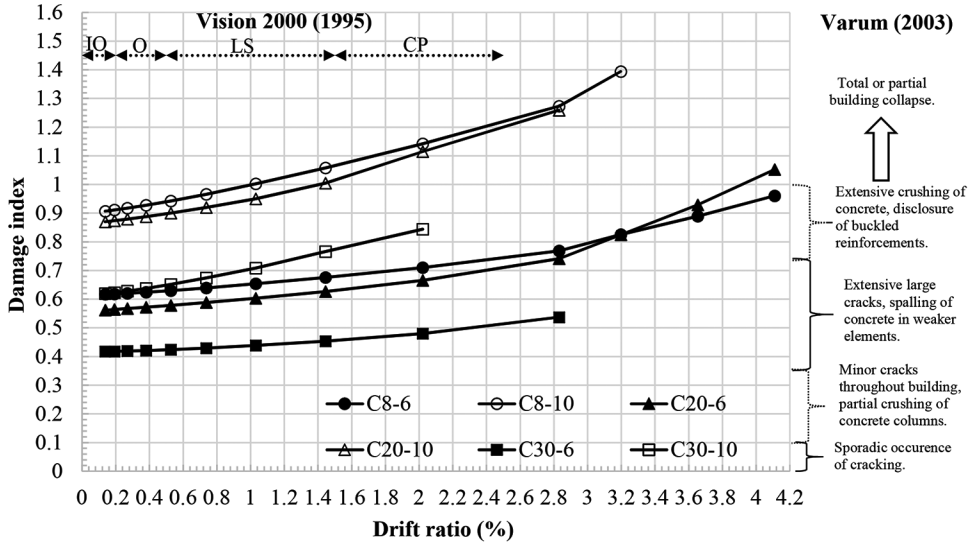


Fig. 16—Damage index.

CONCLUSIONS

The seismic behavior of corroded RC columns under combined cyclic loading was investigated at different concrete strength levels and axial load ratios for detailed gravimetric tests on the corroded reinforcement bars. This study mainly aimed to capture and identify the effects of corrosion level on the structural behavior at different strength levels and axial load ratios by considering both the ascending and descending branches of earthquake indicators. A number of new empirical models for structural engineers were developed. The test results and developed models may provide a guideline for several earthquake codes and further studies. The following conclusions can be drawn based on the obtained experimental test results.

- The yield and ultimate loads of RC columns were slightly increased at lower corrosion levels, and then decreased at higher corrosion levels. Owing to the asymmetric corrosion levels, the structural capacity differed based on the determined unilateral and bilateral failure criteria, where the bilateral criteria exhibited more linear relationships. Considering the present and previous experimental test results, the effects of corrosion on the load-carrying capacity were not significant when the axial load ratio was lower than 0.40. It is conceivable that the lower axial load ratios used in previous studies may be one of the reasons for the contradictions in the literature, through the contribution of corrosion products to the bond strength and slippage of the reinforcement bars in particular, and thus lateral displacement capacity of corroded RC columns.
- In terms of the comparison of previous models, the test results demonstrated that the considered average corrosion levels provided superior performance over the maximum corrosion level for the developed models. This was due to the relationships between the average corrosion levels of the longitudinal bars and stirrups. The corrosion levels obtained according to Faraday's law also resulted in different conclusions for the effects of corrosion on corroded RC columns. If Faraday's law is preferred for considering the corrosion level, it is highly recommended that the actual corrosion levels be obtained at the locations of plastic hinges for further study.
- The authors strongly agree with the conclusion drawn by Li et al. (2018) for the recommendation of using energy dissipation instead of the ductility ratio to assess the seismic performance of corroded RC structures, owing to the increased ductility ratios if bilateral failure criteria are not considered. The authors further underline the importance of the determined damage index of corroded RC columns. The determined damage index, which is also a function of energy dissipation, clearly indicated the corrosion effects, and provides the basis for further study.
- The reduction in the energy dissipation capacity of the corroded RC columns was more significant than other earthquake indicators. It was clearly demonstrated that the test results from bilinear idealized curves of cyclic loops in previous studies caused the aforementioned contradicting results in the literature. Bilinear idealized curves provide yield strength even when the structural members act as brittle. Moreover, they falsely indicate higher ductility for corroded RC columns than non-corroded columns, despite the fact that corroded RC columns absorb less energy prior to failure. Therefore, an energy-based comparison is highly recommended for the determination of the ductility index of corroded RC columns.

AUTHOR BIOS

ACI member **Hakan Yalciner** *is an Associate Professor in the Department of Civil Engineering, Erzincan Binali Yıldırım University, Erzincan, Turkey, and is a Chair of the Structural Research Center at the Corrosion Division. He received his MSc from the European University of Lefke, Lefka, Northen Cyprus, and his PhD from the Eastern Mediterranean University, Famagusta, Northern Cyprus. He is a member of ACI Committee 546, Repair of Concrete, and Subcommittee 546-E, Corrosion Studies. His research interests include the effects of corrosion on structural performance.*

Atila Kumbasaroglu *is an Adjunct Lecturer in the Department of Civil Engineering and a Vice Chair of Research in Corrosion Studies at Erzincan Binali Yıldırım University. He received his MSc and PhD from Atatürk University, Erzurum, Turkey. His research interests include corrosion, composite materials, and structures.*

ACKNOWLEDGMENTS

This research was supported by the Scientific and Technological Council of Turkey, under program TÜBİTAK-3501 (grant number 116M162). The authors wish to express their gratitude and appreciation for the financial support.

NOTATION

E_c = energy dissipation capacity of corroded column
E_o = energy dissipation capacity of non-corroded column
F_{uc} = ultimate load of corroded column
F_{uo} = ultimate load of non-corroded column
F_{yc} = yield load of corroded column
F_{yo} = yield load of non-corroded column
K_{sc} = average normalized secant stiffness of corroded column
K_{so} = average normalized secant stiffness of non-corroded column
Q_y = yield strength when steel bar yields
μ_c = energy ductility index of corroded column
μ_D = displacement ductility ratio
μ_E = energy ductility index
μ_o = energy ductility index of non-corroded column
η = axial load ratio

REFERENCES

AIJ, 1997, "Recommendations for Practice of Survey, Diagnosis and Repair for Deterioration of Reinforced Concrete Structures," Architectural Institute of Japan, Tokyo, Japan.

ASTM G1-03, 2003, "Standard Practice for Preparing, Cleaning, and Evaluating Corrosion Test Specimens," ASTM International, West Conshohocken, PA, 9 pp.

ASTM A370-08a, 2008, "Standard Test Methods and Definitions for Mechanical Testing of Steel Products," ASTM International, West Conshohocken, PA, 47 pp.

Bicer, K.; Yalciner, H.; Pekrioglu Balkıs, A.; and Kumbasaroglu, A., 2018, "Effect of Corrosion on Flexural Strength of Reinforced Concrete Beams with Polypropylene Fibers," *Construction and Building Materials*, V. 185, pp. 574-588. doi: 10.1016/j.conbuildmat.2018.07.021

Cağatay, I. H., 2005, "Experimental Evaluation of Buildings Damaged in Recent Earthquakes in Turkey," *Engineering Failure Analysis*, V. 12, No. 3, pp. 440-452. doi: 10.1016/j.engfailanal.2004.02.007

Di Carlo, F.; Meda, A.; and Rinaldi, Z., 2017, "Numerical Evaluation of the Corrosion Influence on the Cyclic Behaviour of RC Columns," *Engineering Structures*, V. 153, pp. 264-278. doi: 10.1016/j.engstruct.2017.10.020

FEMA 461, 2007, "Interim Testing Protocols for Determining the Seismic Performance Characteristics of Structural and Nonstructural Components," Federal Emergency Management Agency, Washington, DC, pp. 1-113.

Grandić, D., and Bjegović, D., 2011, "Reinforcement Corrosion Rate in Cracked Areas of RC-Members Subjected to Sustained Load," *Modelling of Corroding Concrete Structures*," *RILEM*, V. 5, pp. 65-83.

Guo, A.; Li, H.; Ba, X.; Guan, X.; and Li, H., 2015, "Experimental Investigation on the Cyclic Performance of Reinforced Concrete Piers with Chloride-Induced Corrosion in Marine Environment," *Engineering Structures*, V. 105, pp. 1-11. doi: 10.1016/j.engstruct.2015.09.031

Li, D.; Wei, R.; Xing, F.; Sui, L.; Zhou, Y.; and Wang, W., 2018, "Influence of Non-Uniform Corrosion of Steel Bars on the Seismic Behavior of Reinforced Concrete Columns," *Construction and Building Materials*, V. 167, pp. 20-32. doi: 10.1016/j.conbuildmat.2018.01.149

Liu, X.; Jiang, H.; and He, L., 2017, "Experimental Investigation on Seismic Performance of Corroded Reinforced Concrete Moment-Resisting Frames," *Engineering Structures*, V. 153, pp. 639-652. doi: 10.1016/j.engstruct.2017.10.034

Ma, Y.; Che, Y.; and Gong, J., 2012, "Behavior of Corrosion Damaged Circular Reinforced Concrete Columns under Cyclic Loading," *Construction and Building Materials*, V. 29, pp. 548-556. doi: 10.1016/j.conbuildmat.2011.11.002

Meda, A.; Mostosi, S.; Rinaldi, Z.; and Riva, P., 2014, "Experimental Evaluation of the Corrosion Influence on the Cyclic Behaviour of RC Columns," *Engineering Structures*, V. 76, pp. 112-123. doi: 10.1016/j.engstruct.2014.06.043

Park, Y. J., and Ang, A. H. S., 1985, "Mechanistic Seismic Damage Model for Reinforced Concrete," *Journal of Structural Engineering*, ASCE, V. 111, No. 4, pp. 722-739. doi: 10.1061/(ASCE)0733-9445(1985)111:4(722)

Park, Y. J.; Ang, H. S.; and Wen, Y. K., 1987, "Damage-Limiting Aseismic Design of Buildings," *Earthquake Spectra*, V. 3, No. 1, pp. 1-26. doi: 10.1193/1.1585416

Sezen, H., and Moehle, J. P., 2004, "Strength and Deformation Capacity of Reinforced Concrete Columns with Limited Ductility," *Proceedings of the 13th World Conference on Earthquake Engineering*, V. 279, pp. 1-15.

Shimizu, Y.; Hirosawa, M.; and Zhou, J., 2000, "Statistical Analysis of Concrete Strength in Existing Reinforced Concrete Buildings in Japan," Department Architecture, Faculty of Engineering, Kogakuin University, Tokyo, Japan, pp. 1-88.

Sun, Z.; Si, B.; Wang, D.; and Guo, X., 2008, "Experimental Research and Finite Element Analysis of Bridge Piers Failed in Flexure-Shear Modes," *Earthquake Engineering and Engineering Vibration*, V. 7, No. 4, pp. 403-414. doi: 10.1007/s11803-008-1006-5

Varum, H., 2003, "Seismic Assessment, Strengthening and Repair of Existing Buildings," PhD Thesis, University of Aveiro, Aveiro, Portugal.

Vision 2000, 1995, "Performance Based Seismic Engineering of Buildings," Structural Engineers Association of California, Sacramento, CA.

Yalciner, H.; Eren, O.; and Sensoy, S., 2012b, "An Experimental Study on the Bond Strength Between Reinforcement Bars and Concrete as a Function of Concrete Cover, Strength and Corrosion Level," *Cement and Concrete Research*, V. 42, No. 5, pp. 643-655. doi: 10.1016/j.cemconres.2012.01.003

Yalciner, H.; Kumbasaroglu, A.; Ertuc, İ.; and Turan, A. İ., 2018, "Confinement Effect of Geo-Grid and Conventional Shear Reinforcement Bars Subjected to Corrosion," *Structures*, V. 13, pp. 139-152. doi: 10.1016/j.istruc.2017.12.004

Yalciner, H.; Sensoy, S.; and Eren, O., 2012a, "Time-Dependent Seismic Performance Assessment of a Single-Degree-of-Freedom Frame Subject to Corrosion," *Engineering Failure Analysis*, V. 19, pp. 109-122. doi: 10.1016/j.engfailanal.2011.09.010

Yalciner, H.; Sensoy, S.; and Eren, O., 2015, "Seismic Performance Assessment of a Corroded 50-Year-Old Reinforced Concrete Building," *Journal of Structural Engineering*, ASCE, V. 141, No. 12, pp. 1-11. doi: 10.1061/(ASCE)ST.1943-541X.0001263

Yang, S. Y.; Song, X. B.; Jia, H. X.; Chen, X.; and Liu, X. L., 2016, "Experimental Research on Hysteretic Behaviors of Corroded Reinforced Concrete Columns with Different Maximum Amounts of Corrosion of Rebar," *Construction and Building Materials*, V. 121, pp. 319-327. doi: 10.1016/j.conbuildmat.2016.06.002

Yuan, W.; Guo, A.; and Li, H., 2017, "Experimental Investigation on the Cyclic Behaviors of Corroded Coastal Bridge Piers with Transfer of Plastic Hinge Due to Non-Uniform Corrosion," *Soil Dynamics and Earthquake Engineering*, V. 102, pp. 112-123. doi: 10.1016/j.soildyn.2017.08.019

Yuan, Y.; Ji, Y.; and Shah, S. P., 2007, "Comparison of Two Accelerated Corrosion Techniques for Concrete Structures," *ACI Structural Journal*, V. 104, No. 3, May-June, pp. 344-347.

Zhang, R.; Castel, A.; and François, R., 2009, "Serviceability Limit State Criteria Based on Steel–Concrete Bond Loss for Corroded Reinforced Concrete in Chloride Environment," *Materials and Structures*, V. 42, No. 10, pp. 1407-1421. doi: 10.1617/s11527-008-9460-0

Zhu, W., and François, R., 2014, "Corrosion of the Reinforcement and Its Influence on the Residual Structural Performance of a 26-Year-Old Corroded RC Beam," *Construction and Building Materials*, V. 51, pp. 461-472. doi: 10.1016/j.conbuildmat.2013.11.015